Journal of Materials Chemistry B

ROYAL SOCIETY OF CHEMISTRY

PAPER

View Article Online
View Journal | View Issue

Cite this: J. Mater. Chem. B, 2024, 12, 3774

Static magnetic field enhances the bone remodelling capacity of human demineralized bone matrix in a rat animal model of cranial bone defects†

SeyedJamal Hosseini,‡[ab] Houman Parsaei,‡[c] MirJavad Moosavifar,[abd] Narjes Tavakoli,[e] Reza Ahadi[f] and Kaveh Roshanbinfar *[g]

The regeneration of bone defects that exceed 2 cm is a challenge for the human body, necessitating interventional therapies. Demineralized bone matrices (DBM) derived from biological tissues have been employed for bone regeneration and possess notable osteoinductive and osteoconductive characteristics. Nevertheless, their efficiency in regenerating critically sized injuries is limited, and therefore additional signaling cues are required. Thanks to the piezoelectric properties of the bone, external physical stimulation is shown to accelerate tissue healing. We have implanted human DBM in critically sized cranial bone defects in rat animal models and exposed them to an external magnetic field (1 T) to enhance endogenous bone formation. Our *in vitro* experiments showed the superior cytocompatibility of DBM compared to cell culture plates. Furthermore, alkaline phosphatase activity after 14 days and Alizarin red staining at 28 days demonstrated differentiation of rat bone marrow mesenchymal stem cells into bone lineage on DBM. Computer tomography images together with histological analyses showed that implanting DBM in the injured rats significantly enhanced bone regeneration. Notably, combining DBM transplantation with a 2 h daily exposure to a 1 T magnetic field for 2 weeks (day 7 to 21 post-surgery) significantly improved bone regeneration compared to DBM transplantation alone. This research indicates that utilizing external magnetic stimulation significantly enhances the potential of bone allografts to regenerate critically sized bone defects.

Received 3rd October 2023,
Accepted 16th March 2024

DOI: 10.1039/d3tb02299d

rsc.li/materials-b

Introduction

The principal functions of bone as a connective tissue are mobility, load-bearing, and mechanical support for interior organs. While it has the capacity to regenerate,[1–3] additional treatments and surgical interventions may be required in critically-sized injuries caused by congenital anomalies, tumour resection, or traumatic fracture.[4] Auto-grafting is the gold-standard transplantation therapy. However, the scarcity of donor sites and morbidity in donor sites are significant limitations.[5,6] Tissue engineering is a promising approach for treating critical bone defects and limiting post-operational complications.[7] A three-dimensional (3D) scaffold that resembles the structure and function of bone can facilitate new tissue formation and provide a foundation for bone tissue engineering.[8] Recent advances have significantly fostered bone tissue engineering approaches to generate naturally-derived or synthetic scaffolds with desired characteristics, including osteoconductive ceramics,[9–12] biodegradable synthetic polymers,[13,14] and their composites.[15] Previously, we mimicked the calcium phosphate portion of the bone by generating hydroxyapatite scaffolds for bone tissue

[a] Biomedical Engineering Department, Amirkabir University of Technology, 159163-4311, Tehran, Iran
[b] Cellular and Molecular Research Center, Faculty of Medicine, Iran University of Medical Sciences, 1449614535, Tehran, Iran
[c] Nervous System Stem Cells Research Center, Semnan University of Medical Sciences, 3513138111, Semnan, Iran
[d] Institut für experimentelle molekulare Bildgebung, RWTH Aachen University, Aachen 52074, Germany
[e] School of Industrial Design, College of Fine Arts, University of Tehran, 1415564583, Tehran, Iran
[f] Department of Anatomy, Faculty of Medicine, Iran University of Medical Sciences, 1449614535, Tehran, Iran
[g] Experimental Renal and Cardiovascular Research, Department of Nephropathology, Institute of Pathology, Friedrich-Alexander-Universität Erlangen-Nürnberg (FAU), Erlangen 91058, Germany.
E-mail: Kaveh.Roshanbinfar@uk-erlangen.de; Tel: +499131-8525701

† Electronic supplementary information (ESI) available. See DOI: https://doi.org/10.1039/d3tb02299d

‡ SeyedJamal Hosseini and Houman Parsaei have participated equally in performing research related to this article.

engineering.[11,12,16,17] These biomaterials supported cell attachment and growth. We have recently advanced our approach to generating nanocomposite biomimetic gelatine–calcium phosphate scaffolds to accelerate bone regeneration in rat animal models of critical cranial defects over 90 days.[16] While these approaches resulted in exciting outcomes, they lack a complete resemblance to the native bone extracellular matrix and have limited osteoinductive capacity.[18,19] One alternative is demineralized bone matrix (DBM) which is a composite of collagen (type I, IV, and X), non-collagenous proteins, and growth factors accompanied by a variable percentage of calcium phosphate minerals (1–6%). DBM was identified as such in 1971, resulting in the introduction of the term "osteoinduction".[20] It is a cell-free therapeutic matrix that provides osteoinduction for the appendicular, axial, and craniofacial skeletons.[21] There is a plethora of publications and commercial use of this material confirming its osteoinductiveness.[21] While this material has been used for bone regeneration, its efficiency in treating critically sized bone injuries is limited, necessitating additional combination therapies by introducing signalling cues for such treatments.

Application of external physical stimulations, including laser, ultrasound, and electromagnetic fields, has shown significant enhancement in regenerating skin,[22,23] nervous system,[24,25] and cardiac tissue.[26,27] Among others, there is a wealth of evidence in the literature supporting the beneficial effects of magnetic fields on bone healing.[28,29] Recent research revealed that electromagnetic fields affect cellular calcium, the calcification process, collagen, and proteoglycans within the tissue.[30,31] Electromagnetic fields affect cellular functions and intercellular communications,[32] for example, by increased proliferation, migration, angiogenesis, and differentiation of stem cells into osteoblasts.[33–35] In terms of magnetic intensity, SMF can be categorized as mild ($<$ 1 mT), moderate (1 mT to 1 T), strong (1 T to 5 T), and ultra-strong ($>$ 5T). A wide range of biological systems, especially those closely associated with transmembrane ion flux, have been shown to be sensitive to moderate-intensity static magnetic fields (MSMF), as indicated by a considerable research report.[36] MSMF can influence the phospholipid molecules in the membrane to rotate. It has been documented that the MSMF does not have any inactivation effects on such channels, but rather can affect changes in membrane calcium ion flux. Additionally, exposure to MSMF changes the distribution of osteoblasts and osteoclasts in the callus and significantly affects the bone markers in serum. Furthermore, during the fracture healing process, MSMF exposure has a regulating effect on the iron concentration in the callus and systemic iron metabolism.[37]

We hypothesized that the presence of a static magnetic field (SMF) enhances the bone regeneration capacity of DBM. In this study, DBM was generated from human donors and implanted into critically sized cranial defects (7 mm in diameter circular defects) in a rat animal model. The animals were exposed to the SMF of 1 T for two hours per day for two weeks and bone regeneration was evaluated by computer tomography (CT) and histological analyses.

Results

In vitro effects of magnetic field stimulation

To determine the effects of SMF on cellular activity *in vitro*, rat bone marrow-derived mesenchymal stromal cells (rBMMSCs) were subjected to SMF (two neodymium (Nd2Fe14B) cylindrical magnets with a thickness of 20 mm and diameter of 20 mm; ~0.5 T) for one, three, or seven days (Fig. 1a). At these timepoints, cellular mitochondrial activity was measured based on MTT assay. rBMMSCs stimulated with SMF showed greater mitochondrial activity compared to not stimulated cells (Fig. 1b). Furthermore, the analysis of alkaline phosphatase (ALP) activity at days three and seven revealed that SMF stimulation of rBMMSCs results in greater ALP activity (Fig. 1c). Eventually, the levels of new bone formation were determined based on von Kossa staining at day 14 (Fig. 1d and e). Quantitative analysis of microscopic images of von Kossa staining showed a significant increase in new bone deposition in the cells stimulated by SMF. These data show that SMF stimulation enhances bone commitments in rBMMSCs. Hereafter, we aimed to study the synergistic effects of magnetic field stimulation and the presence of the DBM on bone regeneration.

Successful demineralization and subsequent cell attachment

Demineralized bone matrices were generated from sample biopsies from patients undergoing total hip replacement surgery (Fig. 2a). These samples were cleaned, disinfected, and demineralized after being cut into smaller cubic shapes. To investigate the microstructure of these samples, SEM was performed on the samples of fresh and demineralized bone matrix (Fig. 1b). Analysis of the SEM images revealed the presence of cells on the bone structures that were removed after decellularization and demineralization processes as shown in the SEM images of DBM samples.

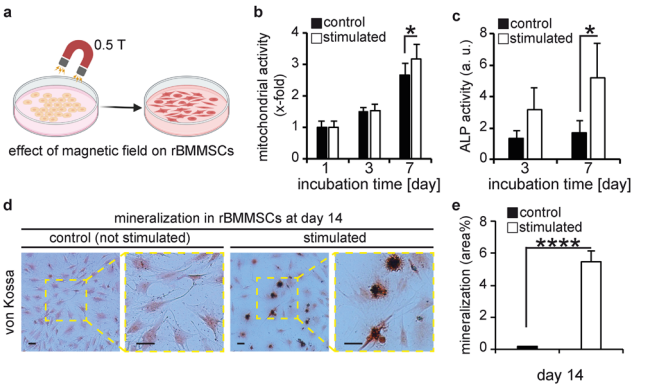

Fig. 1 Static magnetic field stimulation enhances mineralization. (a) Schematic illustration of the magnetic stimulation of rBMMSCs *in vitro*. (b) Quantitative analysis of mitochondrial activity performed based on MTT-assay, correlating with cellular proliferation (N = 3). (c) Quantitative analysis of alkaline phosphatase enzyme activity in rBMMSCs (N = 3). (d) Representative microscopic images of von Kossa staining of rBMMSCs and (e) their quantitative analysis to calculate mineralization in stimulated and non-stimulated cells (N = 3). *: a $p < 0.05$ and ****: $p < 0.0001$. Data are presented as mean ± SD. Scale bars: 100 μm.

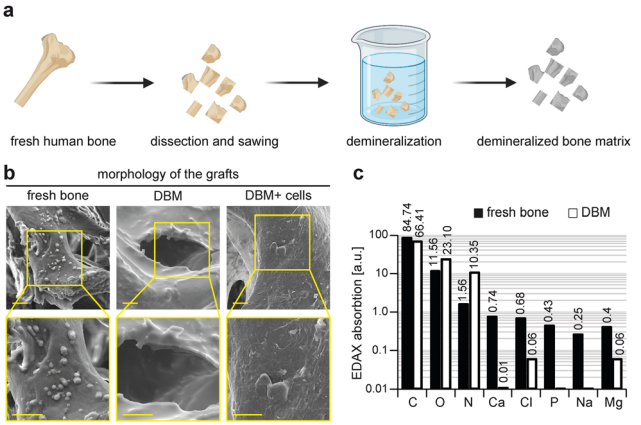

Fig. 2 Characterization of DBM: (a) DBM preparation procedure. (b) SEM images of fresh bone in comparison to DBM allografts illustrating the effectivity of the decellularization process and SEM images of the DBMs at 3 days after seeding rBMMSCs indicating cell attachment on DBM. (c) EDAX elemental analysis of DBM in comparison to fresh bone confirms the demineralization process was efficient in eliminating minerals from grafts. C: carbon, O: oxygen, N: nitrogen, Ca: calcium, Cl: chlorine, P: phosphorous, Na: sodium, and Mg: magnesium. Scale bars: long line: 50 μm, short line: 200 μm.

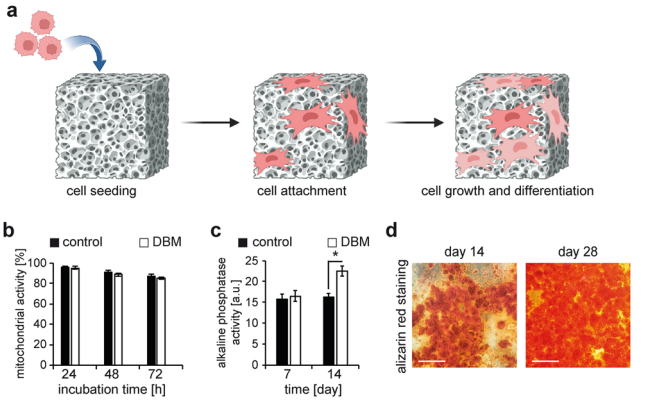

Fig. 3 Characterization of the cell activity. (a) Schematic illustration of cell seeding procedure. (b) Quantitative analysis of mitochondrial activity based on MTT assay (n = 3). (c) Quantitative analysis of alkaline phosphatase (ALP) activity of rBMMSCs cultured on TCPS (control) compared to those on DBM (n = 3). (d) Representative microscopic images of Alizarin red staining demonstrate osteogenic differentiation after 14 and 28 days. * indicates $p < 0.05$ and data are presented as mean ± SD. Scale bars: 20 μm.

To ensure the stability and reproducibility of the generated materials, three samples were independently demineralized and their microstructure was investigated through SEM analysis (Fig. S1, ESI†). SEM images of different samples at multiple magnification levels revealed similar microstructure and morphology of the DBM samples, indicating reproducibility in the generation of matrices. We then tested the cytocompatibility of these grafts by seeding rBMMSCs on DBM samples. These cells were attached to the matrix as detected from SEM images (Fig. 2b). We utilized EDAX analysis to investigate the presence of different elements in fresh and demineralized bone (Fig. 2c).

Quantitative analysis of different elements in the two groups of samples revealed successful removal of calcium phosphate content from bone samples evident by a minimum detection of Ca, P, Na, Cl, and Mg in DBM samples compared to fresh bone.[38]

The SEM images of cell-laden DBM samples confirmed successful cell attachment. We further analysed the mitochondrial activity of these cells at 24, 48, and 72 h and compared them to fresh bone as a control (Fig. 3a and b). There was no significant difference in cellular mitochondrial activity between DBM and cells seeded on tissue culture polystyrene plates (TCPS), indicating that the demineralization process rendered desirable surface characteristics for cells. In order to evaluate whether these scaffolds induce bone differentiation in rBMMSCs, we performed quantitative analysis of the activity of alkaline phosphatase enzyme for the cells cultured on TCPS and DBM scaffolds.

After 7 days, there was no significant difference in ALP activity of cells cultured on TCPS compared to those on DBM scaffolds. However, after two weeks, our data revealed that DBM scaffolds significantly enhanced the ALP activity of these cells, suggesting that DBM scaffolds promote the differentiation of rBMMSCs into bone lineage. We then further evaluated our DBM samples on days 14 and 28 for the efficiency of *in vitro* bone formation by performing Alizarin red staining (Fig. 3d). Our data show a clear increase in the intensity and the surface coverage of the cells stained for Alizarin red. This marker stains calcium deposits in the culture and our data clearly shows enhanced calcium deposition of the rBMMSCs cultured on DBM after 14 and 28 days. These data show that here generated DBM matrices provide a favourable environment for rBMMSCs to differentiate into bone lineage and importantly, deposit calcium.

Our DBM scaffolds showed sufficient support *in vitro* to be utilized for bone regeneration. Hence, we furthered our analysis to evaluate their bone regeneration efficiency *in vivo* in a rat animal model of the critically-sized cranial defect. The goal of these experiments was to identify whether an external SMF enhances the bone regeneration capacity of the DBM grafts in a critically-sized bone defect. Male adult rats were divided into four different groups and a 7 mm circular part of their cranial bone was removed. The generated defects were left empty in two of the groups as a control. One of these two groups was exposed to the 1 T SMF for 2 h per day during the treatment period. The other two experimental groups received DBM grafts in the defect area. One of these groups was also exposed to the same regiment of the SMF that was explained previously. Computer tomography analysis was performed on the animals at days 30, 60, and 90 post-surgery, and Hounsfield numbers were calculated by the machine (Fig. 4). Quantitative analysis of Hounsfield numbers revealed that magnetic field alone enhances bone regeneration in the animals and this regeneration, while not efficient, continues to increase over time. In the absence of a magnetic field, implanting a DBM graft in the defect area significantly enhances bone regeneration in the animals and this enhanced regeneration continues even after 60 and 90 days.

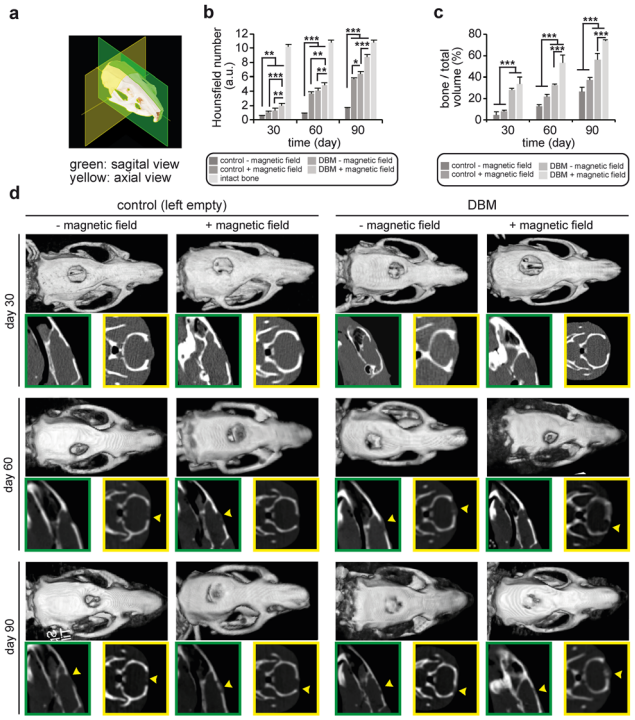

Fig. 4 A combination of static magnetic field and DBM synergistically enhances bone regeneration. (a) Schematic illustrations of sagittal and axial planes. (b) Hounsfield number of samples in the control – magnetic field, control + magnetic field, DBM – magnetic field, and DBM + magnetic field groups at 30, 60, and 90 days post-surgery (n = 3). (c) Quantitative calculations of bone volume over total volume (n = 3) performed based on the CT-images presented in (d) representative images of 3D CT reconstruction and cross-sectioned sagittal (green inserts) and axial (yellow inserts) planes of defect area in the calvarium of the rats in the control – magnetic field, control + magnetic field, DBM – magnetic field, and DBM + magnetic field groups at 30, 60, and 90 days post-surgery. *: a $p < 0.05$, **: $p < 0.01$, ***: $p < 0.001$. Data are presented as mean ± SD.

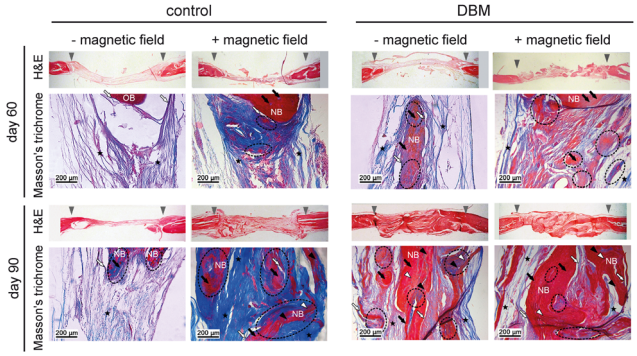

Fig. 5 A combination of magnetic field and DBM transplantation enhances new bone formation. H&E and TCM images of defect areas of rats stained by Haematoxylin and Eosin (H&E) by 10x magnification or Masson's trichrome (TCM) by 40x magnification of the control – magnetic field, control + magnetic field, DBM – magnetic field, and DBM + magnetic field groups at 60 and 90 days post-surgery which confirms osteogenic characteristics of the prepared allografts as well as an enhancing effect of magnetic field exposure. Gray arrowheads in H&E images: initial defect area of 7 mm; OB: old bone; NB: newly formed bone; dashed circle: fibrocartilaginous areas which are being mineralized; black star: fibrous tissue; black arrows: young osteocytes; white arrows: osteoblasts; black arrowheads: lacunae; white arrowheads: collagen fibres.

Additionally, we calculated callus mineralized volume fraction (bone to total volume (BV/TV %)). Similar to Hounsfield numbers, these data showed that the rats receiving DBM and stimulated by SMF had significantly more bone volume with a BV/TV index increased to ~70% in the third month post-implantation, while, the bone volume fraction in control animals with or without magnetic field stimulation remained below 40%.

Interestingly, the combination of DBM implantation and an external SMF of 1 T significantly promotes new bone formation in the defect area. This combination therapy provides a synergy that results in a Hounsfield number equivalent to around 80% of that of the intact bone after 90 days. This level of regeneration was not observed for any of the other experimental groups in our study. To visualize such regeneration, we observed sagittal and axial views of the defect area in all animals at different time points (Fig. 3c). These CT images also confirmed the quantitative data of the Hounsfield numbers discussed above.

In order to further evaluate bone regeneration at the cellular level, histological sections of the defect area were obtained and stained for haematoxylin and eosin (H&E) and Masson's trichrome (Fig. 5). The total defect area was captured in H&E staining images to show the total 7 mm defect area. In these images, bone is visualized by dark pink, and the fibrous tissue by light pink staining. Leaving the defect empty without an external magnetic field resulted in the generation of fibrous tissue without any new bone formation after 60 days. This was slightly improved after 90 days while the histological analysis showed new bone formation in the defect area. Interestingly, when the external magnetic field was exposed to the animals without a graft, new bone formation was detected in the histological staining after 60 days which was significantly improved at day 90. Our data shows that animals receiving DBM grafts exhibited more healing in the defect area. As evident from histological staining images, the amount of new bone formation in the DBM receiving group was significantly more than those that were only exposed to the magnetic field. As expected, the defect size was significantly reduced in groups that received DBM or the combination of DBM and magnetic field therapy. In these two groups, the residual space was filled by newly generated bone. Importantly, denser, more defined, and aligned bone formation was observed for the groups that were exposed to the external 1 T SMF. Notably, the presence of DBM further enhanced these qualities of the newly generated bone in the defect area. In order to distinguish the mineral part from the organic part of the new bone formation in the defect area, the histological sections were stained by Masson's trichrome that stains collagen in blue, mineral parts in red, and the cell nuclei in black. While H&E staining images showed new bone formation in the defect area in the control group exposed to the magnetic field, a closer analysis using Masson's trichrome staining revealed that the majority of this tissue is collagen and thus, it does not provide sufficient mechanical

support to the bone. These animals are also more prone to a repetitive broken bone in the defect area.

The presence of the DBM in the defect area, in confirmation with our *in vitro* data, enhanced the formation of new bone and improved calcium deposition, as shown by Masson's trichrome staining images. Interestingly, the combination of DBM and magnetic field therapy resulted in the best regeneration in which significantly greater amounts of bone minerals were deposited in the defect area, resulting overall in a denser and aligned new bone in the defect area. While previously it has been reported that the magnetic field results in the formation of aligned new bone,[39] we are showing, for the first time, the synergistic enhancement of compact new bone formation in a critically sized bone defect in a DBM and magnetic field combination therapy. The images demonstrate lacunae, collagen fibres, and fibrous areas calcifying to create bone. An aggregation of osteocyte and osteoblasts is defined in the photos.

Discussion

Bone grafts utilizing demineralization techniques have been applied in clinics for more than three decades.[40,41] However, limited advances have been made in order to improve the efficiency of graft-based treatments, especially regarding critically-sized bone defects. These grafts promote bone differentiation and have osteoinductive and osteoconductive characteristics. It has been shown that introducing a magnetic field to the injured bone enhances the regeneration capacity.[42–45] The exact mechanism by which regeneration takes place has not yet been fully determined; however, the interactions of the electromagnetic field with the electroactive bone tissue may be the fundamental cause of the regeneration enhancement.[46,47] Recent studies investigating the impact of SMF on biological systems showed that in addition to the phenotypic alteration of the cytoskeleton and cell adhesion, SMF can affect cell proliferation and differentiation.[48] In terms of mechanism, the effects of SMF on cellular biology might be associated with membrane receptor proteins, intracellular signalling pathways, and other charged molecules like calcium ion signalling pathways.[49,50] Marycz *et al.*[51] showed that SMF can alter ion concentrations in the cytoplasm, particularly Ca^{2+} concentrations, which is consistent with our findings. SMF interacts with Ca^{2+} channels in the cell membrane to regulate the flow of Ca^{2+} ions. In our study, growing calcium deposition in the cells that received 0.5 T SMF was shown by von Kossa staining, indicating an increased cytoplasmic calcium concentration, with further effects on the cells, resulting in changes to the distribution and microdomain of actin. These changes affect the cellular geometry and structure. Furthermore, SMF partially improves bone remodelling through a variety of mechanisms. Yang and colleagues observed a reduction in osteoclasts and TRAP-5B levels in mice exposed to SMF (0.2–0.4 T).[52] In 2021, Lv *et al.*[50] conducted an experiment in which 0.4–0.7 T SMF was administered in mice with type 1 diabetes for four hours each day over a period of six weeks. They showed that the levels of markers for both bone resorption (CTSK and NFAT2) and bone creation (OCN and collagen I) were upregulated. Additionally, SMF increased osteogenesis by elevating ALP levels and mineralization deposition in osteoblasts. Moreover, according to research done in 2020 by Yu Ying's group, 0.2–0.6 T SMF drastically minimized bone loss in mice by encouraging Runx2-mediated gene transcription in BMSCs.[53] Yifan Wang and colleagues carried out another trial in 2022. They investigated how medium-strength SMF and culture media containing Mg^{2+} may encourage the growth and osteogenic differentiation of mesenchymal stem cells from bone marrow. It was discovered that this combination significantly improved osteogenic differentiation and cell proliferation, perhaps through the CREB1 protein and MAGT1 channel.[54] Furthermore, higher levels of osteogenesis-related proteins such as ALP, Collagen I, Osteopontin, and Osteocalcin have been observed in both *in vitro* and *in vivo* after exposure to an external MF.[55]

On the other hand, bone regeneration is a complex and multistage biological process that includes hematoma formation (0–5 days post-injury), fibrocartilaginous callus formation (5–11 days post-injury), bony callus formation (11–28 days post-injury), and bone remodelling (starting at 18 days post-injury and lasting months or years).[56] In the case of critical injuries, the healing process stops at the early stages and fibrous tissue will mainly replace the defect area.[57] This is what we observed in the control groups where the defect was left empty. In order to reach appropriate regeneration, the regenerative cascade must be encouraged to reach the third and fourth stages, where an immature calcified tissue is generated and remodeled.[58] We hypothesized that the initial weeks of bone regeneration are crucial. During this time, a temporary template will emerge before calcification. If the cascade successfully passes this time frame, the process will continue until complete regeneration, provided that external stress does not occur again. Inflammation and hematoma formation, on the other hand, predominate during the first week; accordingly, weeks 2 and 3 post-surgery were chosen as the periods for exposure to the magnetic field, taking into account, according to the timepoints for bone formation discussed above, not only would this period be long enough for effective stimulation, but it would also be short enough to be clinically translatable. Results of our study demonstrate the significance of the early weeks of bone regeneration when implanting a decalcified bone matrix accompanied by only a two-week electromagnetic exposure acting as a winning combination and dramatically boosted the healing rate even up to day 90 post-surgery. The Hounsfield number analysis of bone grafts showed considerable calcium deposition in magnetic field exposure groups over that time, which was near to the intact bone Hounsfield number. Previously it has been shown that short-term ($<$ 4 h per day for 3–10 days) *in vitro* electromagnetic cellular stimulation increases osteoblast proliferation,[38,59] gene expression, protein synthesis,[35] and cellular mineralization.[33] Furthermore, electromagnetic forces have been shown to upregulate the differentiation process[60] and osteogenesis[61] in BMMSCs. In this study, we have shown that these beneficial effects of

magnetic fields can be translated *in vivo* and enhance bone regeneration.

It has been shown that the MSMF of 84.3 Gauss (8.43 mT) enhances bone regeneration when applied to animals receiving neodymium iron boron magnets together with synthetic hydroxyapatite powder or autologous grafts.[62] However, implanting magnetic particles complicates the clinical translation of this approach. Based on this evidence, we decided to recruit an external moderate static magnetic field for our investigation. In another study, Chen *et al.*[63] used sinusoidal electromagnetic fields (1 mT, 15 Hz, 4 h per day) in combination with VEGF growth factor to enhance osteoinduction in 3D printed polylactic acid - hydroxyapatite implants. They demonstrated that sinusoidal electromagnetic fields and VEGF are efficient approaches to enhancing the osteogenesis and vascularization of tissue engineered constructs. Bloise *et al.*[64] found that a pulsed electromagnetic field (2 mT, 75 Hz; pulse duration, 1.3 ms) can improve osteoinductive properties of keratin wool scaffolds *in vitro* in terms of proliferation, differentiation, and production of the calcified bone extracellular matrix. However, compared to our study, the generation of sinusoidal or pulsed electromagnetic fields needs a more complex apparatus, which may not be finally applicable for clinical purposes. Although the effects of electromagnetic fields on other biological functions of the body are still controversial, there is much evidence regarding the positive or neutral effects of exposure of the biological system to SMFs.[65,66]

Furthermore, oriented collagen structure is a key factor in different tissue architectures. Collagen fibres have been found to be organized in a variety of designs, including parallel to a single direction in tendons, a hierarchical structure in cortical bones, and an orthogonal grid in the cornea. In addition, there have been various publications on techniques for orienting collagen fibres *in vitro* as well as strategies for inducing cells to secrete extracellular matrix with an orientated structure. In the bone, collagens have hierarchical structures deposited by osteoblasts in the form of matrix protein that alternately align parallel to and orthogonal to the bone's main stress axis. Mineralization takes place on the collagen scaffold surface as deposits of hydroxyapatite. Therefore, having an extracellular matrix with an oriented structure may lead to better bone mineralization. As an illustrative example, it has been observed that the fibroblasts and bone marrow-derived mesenchymal stem cells growing on the oriented fibres grew in the same direction as the fibres and secreted the oriented extracellular matrix in line with the direction of the fibers.[67] In our findings aligned bone formation was observed for the groups that were exposed to the external 1 T SMF, which, in our opinion, stemmed from oriented collagen fibres. The presence of the DBM in the defect area accompanied by the magnetic field, in confirmation with our *in vitro* and *in vivo* data, enhanced the formation of new bone and improved calcium deposition, as shown by Masson's trichrome staining images and the Hounsfield number equivalent to around 80% of that of the intact bone after 90 days. Therefore, new bone was denser in the group in which bone matrix implantation received SMF.

Conclusion

Collectively, in this study, we successfully prepared allograft substitutes for bone tissue engineering with favourable osteoinductive properties. Secondly, we proved that magnetic stimulation, even for a brief time following surgery (2 h per day for 14 days), can substantially augment bone formation in the defect area.

Experimental section

Preparation of allografts

Following total hip replacement, raw tissue was harvested from the femur head of two donors (age 59 and 66 years, male) after receiving their full ethical consent to use their tissue in research and laboratory investigations. Until undertaking serological and polymerase chain reaction (PCR) tests, the tissues were kept in −80 °C freezer. They were then allowed to thaw overnight at 4 °C and any soft tissue and cartilage remnants were removed using sterile surgical instruments. The cancellous regions were cut into 1 cm^3 cubes using a sagittal saw (Aesculap, Germany), and each donor's cubes were placed in separate sterile beakers, washed, and decellularized according to the previously described procedure with some modifications.[68,69] Bone cubes were immersed in pre-heated distilled water at 53–59 °C and sonicated for 15 min at 40 kHz (Decon sonication water bath). Allografts were rinsed in phosphate-buffered saline (PBS – Sigma Aldrich, USA), washed in pre-heated distilled water at 53–59 °C on an orbital shaker at 200 rpm, and centrifuged at 1850 g for 15 min at room temperature. This procedure was repeated two more times each for 10 min. Next, allografts were sonicated at 40 kHz in a solution of 3% (v/v) hydrogen peroxide (Merck, Germany) for 10 min, followed by a wash in 100% (v/v) ethanol (Merck, Germany) on an orbital shaker (70 rpm) at room temperature overnight. Allografts were then submerged in 70% (v/v) ethanol (Merck, Germany) and then in distilled water at 53–59 °C, each for 10 min on an orbital shaker and subsequently centrifuged at 1850 g at room temperature for 15 min. The last two steps were repeated twice. Decellularization was finished by placing allografts in distilled water at room temperature for 30 min on an orbital shaker. Acid demineralization was done at a ratio of 1 g bone: 50 mL of 0.5 N HCl (Fluka). To prevent floating grafts on the surface of the solution due to CO_2 release, they were trapped in autoclaved polymeric baskets in advance. A magnetic stirring plate was used to spin the acid continuously at 500 rpm. Bone cubes were demineralized for 24 h. After demineralization was complete, the acid was poured out, and then distilled water was added and constantly stirred for 20 min. Serial washing steps with water, PBS, water, and water were performed under stirring at 500 rpm. The pH was neutralized and washed in distilled water. Before the final water wash was discarded, the DBM sponges were gently squeezed between fingers to remove excess water. This also served as a manual test for demineralization because any significant calcium deposits would hinder the cube from being compressed completely. After compression, cubes were observed to recover their original sizes. After that, the bone was kept frozen at

−40 °C for future experiments. Before being employed for *in vitro* and *in vivo* experiments, the prepared samples were stored in a cool and dry place. At the end, the bone cubes were cut into tablet-shaped disks with 7 mm diameter and 0.5 mm thickness, sterilized under UV exposure for 40 min, and then washed with PBS and distilled water before being exploited for each biological test.

Morphology of the allograft scaffold

Micrographs of the prepared allografts as well as fresh bones were obtained *via* scanning electron microscopy (SEM) after being freeze-dried using an Alpha 1–2 LD Plus freeze-drier (Christ, Germany) and gold coated by K450X sputter coater (EMI-TECH, England). A Philips XL30 CP microscope was used to take micrographs at an acceleration voltage of 15 kV. Additionally, the reproducibility and the stability of the materials were assessed by means of a SEM (FEIESEM QUANTA 200) at an acceleration of 25 kV.

Energy-dispersive X-ray spectroscopy

The chemical composition of the prepared grafts and fresh bone was analysed *via* energy-dispersive X-ray spectroscopy (EDAX) based on our previously reported work.[70] After freeze drying, allografts and fresh bone were coated with gold and examined using a Philips XL 30 CP SEM, which was operated at 20 kV and 0.78 kCPS.

Cell culture studies

For *in vitro* tests, the extraction of rat bone marrow mesenchymal stem cells (rBMMSCs) was performed according to the previously mentioned procedure.[16] An 8-week-old rat was sacrificed according to the ethics committee guidelines for laboratory animals approved by the Iran University of Medical Sciences (Tehran, Iran). Afterward, prior to flushing bone marrow by Dulbecco's Modified Eagle Medium (DMEM – Sigma Aldrich, USA) supplemented by 1% penicillin/streptomycin (Sigma Aldrich, USA) and 1% L-glutamine (Sigma Aldrich, USA), the cancellous bone detached from the femur and tibia and was washed 3 to 5 times with PBS. The remaining cells were then transferred into a 25 cm^2 culture flask containing DMEM with 10% (v/v) fetal bovine serum (FBS, Sigma Aldrich, USA) and incubated at 37 °C and 5% CO_2. The floating cells were removed after overnight incubation, and then the culture medium was renewed twice a week until the third passage.

Cell proliferation assay

The rBMMSCs (5×10^3 cell mL^{-1}) were cultured on separate sterile 96-well plates (SPL, South Korea) with or without SMF in order to explore the impact of SMF on cell proliferation. The plates were then incubated in a standard cell culture incubator for up to 72 h. Following that, 100 μL of MTT solution (5 mg mL^{-1} in PBS) was added to each well and incubated for three hours to evaluate the cell viability at 24, 48, and 72 h. The formazan precipitates were dissolved in isopropyl alcohol after the MTT solution was removed, and each sample's absorbance was measured at 570 nm using an ELISA reader (ELX808, BioTek).

Von Kossa staining

SMF-related mineralization was evaluated by von Kossa staining. rBMMSCs were cultured on two separate sterile 6-well plates (SPL, South Korea). The DMEM medium containing 10% (v/v) fetal bovine serum (FBS, Sigma Aldrich, USA) was renewed every 3 days. Over a period of seven days, one of the plates was surrounded by magnetic fields produced by 0.5 T neodymium magnets, while the other was isolated from any magnetic fields. At the end of 7 days, Von Kossa staining was carried out; according to Borciani *et al.*,[71] the culture medium was removed, and the cell layers received a PBS wash. The cell layers were then fixed for five minutes with ice-cooled methanol kept at −20 °C. After that, the cells were washed with PBS 1× wash. The cells were then stained, as follows: A 2% $AgNO_3$ solution was added for 1 h at room temperature in the presence of light and then rinsed twice with distilled water. Next, the cell layers were soaked with a 2.5% sodium thiosulfate solution for 5 min and washed with distilled water. Finally, the cells were subjected to a 0.33% neutral red solution for 1 h.

Bone biomarker assay

In order to analyse the impact of SMF on bone biomarker secretion, an ALP assay was carried out on the cells that received 0.5 T SMF. An alkaline phosphatase activity kit (Man Co., Iran) was utilized to measure the ALP release after 3-day and 7-day exposure to SMF. Briefly, 3×10^5 cells were seeded on the 6-well plates and cultured for 3 or 7 days in the magnetic fields. The culture medium was removed, and the cells were rinsed once with PBS. Then, the cell lysis was carried out with a solution of 0.2% Triton X-100 in purified water by shaking for 20 min at room temperature. Finally, ALP activity was measured according to the manufacturer's protocol.

Cell viability test

In order to evaluate the cytocompatibility of the generated scaffolds, [4,5-dimethylthiazol-2-yl]-2,5-diphenyltetrazolium bromide (MTT, Sigma Aldrich, USA) assay was performed to quantitatively analyse the mitochondrial activity of the cells. Based on our previously reported work with slight modification,[72] rBMMSCs (5×10^3 cell mL^{-1}) were seeded on either the sterile sample of allografts or Tissue Culture Polystyrene (TCPS) as a control in a pre-sterilized 96 well plate (SPL, South Korea). Cells and samples were then incubated for up to 72 h in a standard cell culture incubator. In order to assess the cell viability at 24, 48, and 72 h post seeding, 100 μL MTT solution (5 mg ml^{-1} in PBS) was added to each well and incubated for three hours. After removing the MTT solution, the formazan precipitates were dissolved in isopropyl alcohol, and the absorbance of each sample was read at 570 nm *via* an ELISA reader (ELX808, BioTek).[73]

Cell morphology analysis

On day 3 of incubation, the morphology of rBMMSCs seeded on allografts was examined by SEM (Philips XL30 microscope) at a

15 kV acceleration voltage. Cells were fixed using a 4% paraformaldehyde solution in PBS, and then the samples were washed with PBS, dehydrated in a 20–100% ethanol series, and dried in hexamethyldisilazane for 20 min before being stored in a desiccator. The samples were eventually gold coated using a sputter coater and then imaged *via* SEM.

Alkaline phosphatase activity assay

In order to assess the formation of new bone, alkaline phosphatase (ALP) activity was quantified using an Alkaline Phosphatase Activity Kit (Abcam, UK). This kit based on the hydrolysis of *p*-nitrophenyl phosphate to *p*-nitrophenol was utilized.[74] Briefly, 3×10^5 cells were seeded on allografts and cultured for 7 or 14 days. The culture medium was removed and cells were rinsed once with PBS. Then, radio-immunoprecipitation assay lysis buffer (RIPA, 200 μL Chem Cruz, USA) and phenylmethylsulfonyl fluoride protease inhibitor (PMSF, 2 μl, Fisher Scientific, USA) were added to generate cell lysate by shaking at 4 °C. Finally, ALP activity was measured according to the manufacturer's protocol.

Alizarin red staining

The formation of calcium phosphate minerals by rBMMSCs was revealed by the Alizarin red S staining. In six-well plates, 3×10^5 cells were seeded on samples and cultured for 14 and 28 days. The culture medium was aspirated prior to three rounds of PBS rinsing. Then, cells were fixed in formaldehyde solution (3.6%) for 15 min at room temperature. Staining was performed by incubating alizarin red S solution (2% w/v, pH 4.1–4.3) with the cells for 15 min at room temperature before being washed with distilled water. A Nikon TS-100 microscope was then used for microscopy.

Surgical procedure

For *in vivo* experiments, 24 male adult Wistar rats (200–250 g) were used with all the procedures being performed after approval of the ethics committee for laboratory animals in the Iran University of Medical Sciences (Ethical Code: IR.IUMS.FMD.REC.1400.338). To make critical defects, after anesthetizing the animals with Ketamine hydrochloride (90 mg kg^{-1}) and Xylazine (10 mg kg^{-1}), the surgery area was shaved, and the cranium was exposed by making an incision along the midline skin. Then, using an electrical trephine (NST, Japan), a 7 mm circular defect was created, and the remaining bone was removed with care.

Four groups (n = 6) were defined, control − magnetic field, control + magnetic field, DBM − magnetic field, and DBM + magnetic field. In the control − magnetic field and control + magnetic field groups, the defects were left empty, and in the DBM − magnetic field and DBM + magnetic field groups, the defects were filled with disk-shaped allografts (1 mm thick, 7 mm in diameter). While + magnetic field groups were exposed to a SMF, −magnetic field groups were allowed to live normally until further investigations were planned.

Magnetic field exposure

A specifically designed apparatus was built to investigate the effects of a magnetic field on the samples. Fig. 6 shows a schematic of the device; in brief, a non-magnetic substance (PMMA) was used to fix two identical square ferrite magnets installed parallel to each other at a distance of 10 cm. The magnets strength and their distance were adjusted in order to achieve a magnetic flux of 1 T at the centreline of the gap between the two magnets. From day 7 to day 21 after surgery, rats from the control + magnetic field and DBM + magnetic field groups were given general anaesthesia and exposed to a 1 T magnetic field for two hours on a daily basis (duration of two weeks). An equal dose of anaesthesia was administered to the magnetic field groups, but they were not exposed to any magnetic fields.

3D computed tomography

3D computed tomographs (CT) were obtained *via* either the "Siemens SOMATOM Definition AS" or "Siemens SOMATOM Emotion 16 Eco" CT-scanner set at (80 kV, 60 mAs, Interval: Zero) at 30, 60, and 90 days after surgery. Rats received general anaesthesia and the evaluation was triplicated for each group (n = 3). As shown in the formula below, Hounsfield Numbers were also determined and normalized by comparison with the Hounsfield Number of each rat's calvarium in order to assess the density of neo-tissue in the area of injury. Additionally, an allograft sample's Hounsfield number was measured to ensure that it would not mislead the calculations.

$$H = H_d/H_c \times 1000 \quad (1)$$

where H is the relative Hounsfield number, H_d is the Hounsfield number in the defect area, and H_c is the Hounsfield number of the sample rat's calvarial bone. The ratio of callus bone volume over total volume was calculated using NIH ImageJ based on the CT-images.

Histological analysis

In order to analyse the histological parameters of the defected areas at 60 and 90 days, after the euthanasia of the rats, the

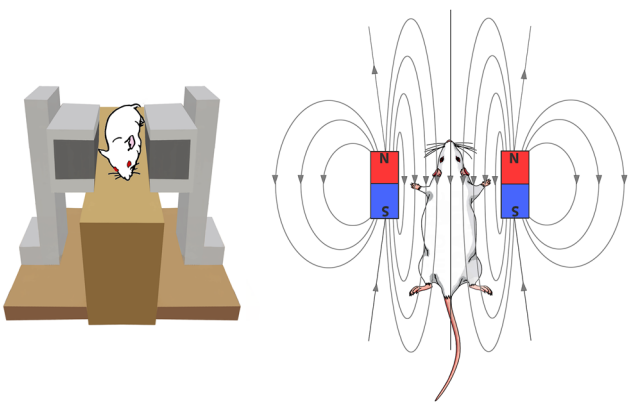

Fig. 6 Schematic of apparatus designed to expose the samples to a magnetic field.

defected area and its surrounding intact bones were cut, and soft tissue remnants were extracted. Afterward, fixation was performed in 4% paraformaldehyde followed by dehydration for 72 h in ethanol series and decalcification in 1% HCl solution for 35 days. The samples were then embedded in paraffin blocks and microtome serial sections with a thickness of 5 μm were created. Prior to the histological examination of random sections of each sample *via* a light microscope (Zeiss, Germany), they were stained with either Haematoxylin and Eosin (H&E) or Masson's trichrome in accordance with the manufacturer's protocol (Far test, Iran).

Statistical analyses

Whenever not mentioned, the experiments were repeated three times. SPSS software (ver 22) was utilized to compare data in a one-way analysis of variance (ANOVA). The results are presented as mean ± standard deviation (SD).

Author contributions

K. R. and SJ. H.: concept and design, project administration, validation of analytical methods, manuscript writing, final manuscript approval; H. P.: conception and design, research implementation, final approval of the manuscript; M. J. M. and R. A.: writing the original draft of the manuscript, data analysis, final approval of the manuscript; N. T. contributed to the manuscript writing, prepared the figures and graphical abstract, data analysis, and final approval of the manuscript.

Conflicts of interest

The authors declare no conflict of interest.

Acknowledgements

Authors would like to acknowledge Preclinical Lab, Core Facility, Tehran University of Medical Sciences, Tehran, Iran for providing the image processing service as well as Mrs Bita Kohnavard from Cellular and Molecular Research Center in Iran University of Medical Sciences, Tehran, Iran for her assistance with cell culture. This research was funded by Universitätsklinikum Erlangen ELAN IZKF, grant number P093/Aktenzeichen: 21-05-20-1-Roshanbinfar.

References

1 S. P. Soundarya, A. H. Menon, S. V. Chandran and N. Selvamurugan, Bone tissue engineering: Scaffold preparation using chitosan and other biomaterials with different design and fabrication techniques, *Int. J. Biol. Macromol.*, 2018, **119**, 1228–1239.
2 S. Saravanan, R. Leena and N. Selvamurugan, Chitosan based biocomposite scaffolds for bone tissue engineering, *Int. J. Biol. Macromol.*, 2016, **93**, 1354–1365.
3 D. Tang, R. S. Tare, L.-Y. Yang, D. F. Williams, K.-L. Ou and R. O. Oreffo, Biofabrication of bone tissue: approaches, challenges and translation for bone regeneration, *Biomaterials*, 2016, **83**, 363–382.
4 L. Li, H. Lu, Y. Zhao, J. Luo, L. Yang, W. Liu and Q. He, Functionalized cell-free scaffolds for bone defect repair inspired by self-healing of bone fractures: A review and new perspectives, *Mater. Sci. Eng., C*, 2019, **98**, 1241–1251.
5 R. Pollock, I. Alcelik, C. Bhatia, G. Chuter, K. Lingutla, C. Budithi and M. Krishna, Donor site morbidity following iliac crest bone harvesting for cervical fusion: a comparison between minimally invasive and open techniques, *Eur. Spine J.*, 2008, **17**, 845–852.
6 Y. Khan, M. J. Yaszemski, A. G. Mikos and C. T. Laurencin, Tissue engineering of bone: material and matrix considerations, *Jbjs*, 2008, **90**, 36–42.
7 R. LogithKumar, A. KeshavNarayan, S. Dhivya, A. Chawla, S. Saravanan and N. Selvamurugan, A review of chitosan and its derivatives in bone tissue engineering, *Carbohydr. Polym.*, 2016, **151**, 172–188.
8 L. Polo-Corrales, M. Latorre-Esteves and J. E. Ramirez-Vick, Scaffold design for bone regeneration, *J. Nanosci. Nanotechnol.*, 2014, **14**(1), 15–56.
9 P. Diaz-Rodriguez, M. López-Álvarez, J. Serra, P. González and M. Landín, Current stage of marine ceramic grafts for 3D bone tissue regeneration, *Mar. Drugs*, 2019, **17**(8), 471.
10 Y. Wen, S. Xun, M. Haoye, S. Baichuan, C. Peng, L. Xuejian, Z. Kaihong, Y. Xuan, P. Jiang and L. Shibi, 3D printed porous ceramic scaffolds for bone tissue engineering: a review, *Biomater. Sci.*, 2017, **5**(9), 1690–1698.
11 J. Hoseini, G. Kaka, S. H. Sadraie and K. Roshanbinfar, Fabrication of variable porous hydroxyapatite scaffolds to investigate appropriate mechanical and morphological properties for bone tissue engineering, *J. Biomater. Tissue Eng.*, 2014, **4**(2), 138–142.
12 S. H. Sadraie, K. Roshanbinfar, G. Kaka and J. Hoseini, Mechanical and structural study of hydroxyapatite (HA) scaffolds produced by gel casting and sponge replication methods, *J. Biomater. Tissue Eng.*, 2014, **4**(7), 562–566.
13 A. Marino, C. Filippeschi, G. G. Genchi, V. Mattoli, B. Mazzolai and G. Ciofani, The Osteoprint: a bioinspired two-photon polymerized 3-D structure for the enhancement of bone-like cell differentiation, *Acta Biomater.*, 2014, **10**(10), 4304–4313.
14 A. Marino, J. Barsotti, G. De Vito, C. Filippeschi, B. Mazzolai, V. Piazza, M. Labardi, V. Mattoli and G. Ciofani, Two-photon lithography of 3D nanocomposite piezoelectric scaffolds for cell stimulation, *ACS Appl. Mater. Interfaces*, 2015, **7**(46), 25574–25579.
15 E. Sharifi, M. Azami, A.-M. Kajbafzadeh, F. Moztarzadeh, R. Faridi-Majidi, A. Shamousi, R. Karimi and J. Ai, Preparation of a biomimetic composite scaffold from gelatin/collagen and bioactive glass fibers for bone tissue engineering, *Mater. Sci. Eng., C*, 2016, **59**, 533–541.
16 M. Moosavifar, H. Parsaei, S. Hosseini, S. M. Mirmontazeri, R. Ahadi, S. Ahadian, F. B. Engel and K. Roshanbinfar,

Biomimetic Organic–Inorganic Nanocomposite Scaffolds to Regenerate Cranial Bone Defects in a Rat Animal Model, *ACS Biomater. Sci. Eng.*, 2022, **8**(3), 1258–1270.

17 K. Roshanbinfar and M. Ansari, Investigating of mechanical and biological properties of porous hydroxyapatite scaffolds produced by novel shake gel casting method, *J. Biomater. Tissue Eng.*, 2013, **3**(3), 284–288.

18 A. J. Salgado, O. P. Coutinho and R. L. Reis, Bone tissue engineering: state of the art and future trends, *Macromol. Biosci.*, 2004, **4**(8), 743–765.

19 M. Bouyer, R. Guillot, J. Lavaud, C. Plettinx, C. Olivier, V. Curry, J. Boutonnat, J.-L. Coll, F. Peyrin and V. Josserand, Surface delivery of tunable doses of BMP-2 from an adaptable polymeric scaffold induces volumetric bone regeneration, *Biomaterials*, 2016, **104**, 168–181.

20 D. Chen, M. Zhao and G. R. Mundy, Bone morphogenetic proteins, *Growth Factors*, 2004, **22**(4), 233–241.

21 E. Gruskin, B. A. Doll, F. W. Futrell, J. P. Schmitz and J. O. Hollinger, Demineralized bone matrix in bone repair: history and use, *Adv. Drug Delivery Rev.*, 2012, **64**(12), 1063–1077.

22 J. Voigt, M. Wendelken, V. Driver and O. M. Alvarez, Low-frequency ultrasound (20-40 kHz) as an adjunctive therapy for chronic wound healing: a systematic review of the literature and meta-analysis of eight randomized controlled trials, *Int. J. Low Extrem. Wounds*, 2011, **10**(4), 190.

23 G. Tai, M. Tai and M. Zhao, Electrically stimulated cell migration and its contribution to wound healing, *Int. J. Burns Trauma*, 2018, **6**, 20.

24 L. Ghasemi-Mobarakeh, M. P. Prabhakaran, M. Morshed, M. H. Nasr-Esfahani, H. Baharvand, S. Kiani, S. S. Al-Deyab and S. Ramakrishna, Application of conductive polymers, scaffolds and electrical stimulation for nerve tissue engineering, *J. Tissue Eng. Regener. Med.*, 2011, **5**(4), e17–35.

25 J. Huang, X. Hu, L. Lu, Z. Ye, Q. Zhang and Z. Luo, Electrical regulation of Schwann cells using conductive polypyrrole/chitosan polymers, *J. Biomed. Mater. Res., Part A*, 2010, **93**(1), 164–174.

26 W. L. Stoppel, D. L. Kaplan and L. D. Black III, Electrical and mechanical stimulation of cardiac cells and tissue constructs, *Adv. Drug Delivery Rev.*, 2016, **96**, 135–155.

27 F. Xie and C. W. Zemlin, Effect of twisted fiber anisotropy in cardiac tissue on ablation with pulsed electric fields, *PLoS One*, 2016, **11**(4), e0152262.

28 J. Zhang, C. Ding, L. Ren, Y. Zhou and P. Shang, The effects of static magnetic fields on bone, *Prog. Biophys. Mol. Biol.*, 2014, **114**(3), 146–152.

29 S. Xu, H. Okano, N. Tomita and Y. Ikada, Recovery effects of a 180 mT static magnetic field on bone mineral density of osteoporotic lumbar vertebrae in ovariectomized rats, *J. Evidence-Based Complementary Altern. Med.*, 2010, 2011.

30 L. A. Norton and L. A. Rovetti, Calcium incorporation in cultured chondroblasts perturbed by an electromagnetic field, *J. Orthop. Res.*, 1988, **6**(4), 559–566.

31 R. K. Aaron, D. M. Ciombor and G. Jolly, Stimulation of experimental endochondral ossification by low-energy pulsing electromagnetic fields, *J. Bone Miner. Res.*, 2020, **4**(2), 227–233.

32 M. Rohde, J. Ziebart, T. Kirschstein, T. Sellmann, K. Porath, F. Kühl, B. Delenda, C. Bahls, U. van Rienen and R. Bader, Human osteoblast migration in DC electrical fields depends on store operated Ca^{2+}-release and is correlated to upregulation of stretch-activated TRPM7 channels, *Front. Bioeng. Biotechnol.*, 2019, **7**, 422.

33 L. Suryani, J. H. Too, A. M. Hassanbhai, F. Wen, D. J. Lin, N. Yu and S.-H. Teoh, Effects of electromagnetic field on proliferation, differentiation, and mineralization of MC3T3 cells, *Tissue Eng., Part C*, 2019, **25**(2), 114–125.

34 H. Y. Lin and Y. J. Lin, In vitro effects of low frequency electromagnetic fields on osteoblast proliferation and maturation in an inflammatory environment, *Bioelectromagnetics*, 2011, **32**(7), 552–560.

35 M. T. Tsai, W. H. S. Chang, K. Chang, R. J. Hou and T. W. Wu, Pulsed electromagnetic fields affect osteoblast proliferation and differentiation in bone tissue engineering, *Bioelectromagnetics*, 2007, **28**(7), 519–528.

36 A. D. Rosen, Mechanism of action of moderate-intensity static magnetic fields on biological systems, *Cell Biochem. Biophys.*, 2003, **39**, 163–173.

37 S. Wang, Y. Liu, C. Lou, C. Cai, W. Ren, J. Liu, M. Gong, P. Shang and H. Zhang, Moderate static magnetic field promotes fracture healing and regulates iron metabolism in mice, *Biomed. Eng.*, 2023, **22**(1), 107.

38 Y. Wei, H. Xiaolin and S. Tao, Effects of extremely low-frequency-pulsed electromagnetic field on different-derived osteoblast-like cells, *Electromagn. Biol. Med.*, 2008, **27**(3), 298–311.

39 H. Kotani, H. Kawaguchi, T. Shimoaka, M. Iwasaka, S. Ueno, H. Ozawa, K. Nakamura and K. Hoshi, Strong static magnetic field stimulates bone formation to a definite orientation in vitro and in vivo, *J. Bone Miner. Res.*, 2002, **17**(10), 1814–1821.

40 N. Shibuya and D. C. Jupiter, Bone graft substitute: allograft and xenograft, *Clin. Podiatric Med. Surg.*, 2015, **32**(1), 21–34.

41 M. Liu and Y. Lv, Reconstructing bone with natural bone graft: a review of in vivo studies in bone defect animal model, *Nanomaterials*, 2018, **8**(12), 999.

42 O. Topal, M. Çina Aksoy, İ. M. Ciriş, D. K. Doğuç, S. Sert and S. Çömlekçi, Assessment of the effect of pulsed electromagnetic field application on the healing of bone defects in rats with heparin-induced osteoporosis, *Electromagn. Biol. Med.*, 2020, **39**(3), 206–217.

43 S. Liu, J. Bi, Y. Zhang, Q. Song, M. Yu, X. Sun, D. Qu and S. Liu, Preliminary study on the electromagnetic field treatment of osteoporosis in rats, *Technol. Health Care*, 2020, **28**(S1), 47–55.

44 C. Daish, R. Blanchard, K. Fox, P. Pivonka and E. Pirogova, The application of pulsed electromagnetic fields (PEMFs) for bone fracture repair: past and perspective findings, *Ann. Biomed. Eng.*, 2018, **46**, 525–542.

45 H. Mohajerani, F. Tabeie, F. Vossoughi, E. Jafari and M. Assadi, Effect of pulsed electromagnetic field on mandibular

fracture healing: A randomized control trial, (RCT), *J. Stomatol. Oral Maxillofac. Surg.*, 2019, **120**(5), 390–396.

46 J. Yuan, F. Xin and W. Jiang, Underlying signaling pathways and therapeutic applications of pulsed electromagnetic fields in bone repair, *Cell. Physiol. Biochem.*, 2018, **46**(4), 1581–1594.

47 B. Zhang, Y. Xie, Z. Ni and L. Chen, Effects and mechanisms of exogenous electromagnetic field on bone cells: a review, *Bioelectromagnetics*, 2020, **41**(4), 263–278.

48 J. Wang and P. Shang, Static magnetic field: A potential tool of controlling stem cells fates for stem cell therapy in osteoporosis, *Prog. Biophys. Mol. Biol.*, 2023, **178**, 91–102.

49 C.-Y. Chang, W.-Z. Lew, S.-W. Feng, C.-L. Wu, H.-H. Wang, S.-C. Hsieh and H.-M. Huang, Static magnetic field-enhanced osteogenic differentiation of human umbilical cord-derived mesenchymal stem cells via matrix vesicle secretion, *Int. J. Radiat. Biol.*, 2020, **96**(9), 1207–1217.

50 H. Lv, Y. Wang, C. Zhen, J. Liu, X. Chen, G. Zhang, W. Yao, H. Guo, Y. Wei and S. Wang, A static magnetic field improves bone quality and balances the function of bone cells with regulation on iron metabolism and redox status in type 1 diabetes, *FASEB J.*, 2023, **37**(7), e22985.

51 K. Marycz, K. Kornicka and M. Röcken, Static magnetic field (SMF) as a regulator of stem cell fate–new perspectives in regenerative medicine arising from an underestimated tool, *Stem Cell Rev. Rep.*, 2018, **14**, 785–792.

52 J. Yang, S. Zhou, H. Lv, M. Wei, Y. Fang and P. Shang, Static magnetic field of 0.2–0.4 T promotes the recovery of hindlimb unloading-induced bone loss in mice, *Int. J. Radiat. Biol.*, 2021, **97**(5), 746–754.

53 G. Chen, Y. Zhuo, B. Tao, Q. Liu, W. Shang, Y. Li, Y. Wang, Y. Li, L. Zhang and Y. Fang, Moderate SMFs attenuate bone loss in mice by promoting directional osteogenic differentiation of BMSCs, *Stem Cell Res. Ther.*, 2020, **11**, 1–14.

54 Y. Wang, X. Wu, W. Yang, P. Feng, W. Tan, Y. Deng and C. Shuai, Magnesium–magnetic field synergy enhances mouse bone marrow mesenchymal stem cell differentiation into osteoblasts via the MAGT1 channel, *J. Nanomater.*, 2022, 2022.

55 Y.-Z. Zhao, R. Chen, P.-P. Xue, L.-Z. Luo, B. Zhong, M.-Q. Tong, B. Chen, Q. Yao, J.-D. Yuan and H.-L. Xu, Magnetic PLGA microspheres loaded with SPIONs promoted the reconstruction of bone defects through regulating the bone mesenchymal stem cells under an external magnetic field, *Mater. Sci. Eng., C*, 2021, **122**, 111877.

56 J. R. Sheen; A. Mabrouk and V. V. Garla, Fracture Healing Overview. In StatPearls, StatPearls Publishing Copyright © 2024, StatPearls Publishing LLC.: Treasure Island (FL) ineligible companies. Disclosure: Ahmed Mabrouk declares no relevant financial relationships with ineligible companies. Disclosure: Vishnu Garla declares no relevant financial relationships with ineligible companies., 2024.

57 D. Smrke; P. Rožman; M. Veselko and B. Gubina, in Treatment of bone defects—allogenic platelet gel and autologous bone technique, *Regenerative medicine and tissue engineering*, IntechOpen, 2013.

58 E. Roddy, M. R. DeBaun, A. Daoud-Gray, Y. P. Yang and M. J. Gardner, Treatment of critical-sized bone defects: clinical and tissue engineering perspectives, *Eur. J. Ortho. Surg. Traumatol.: Ortho. Traumatol.*, 2018, **28**, 351–362.

59 H. Miyamoto, Y. Sawaji, T. Iwaki, T. Masaoka, E. Fukada, M. Date and K. Yamamoto, Intermittent pulsed electromagnetic field stimulation activates the mTOR pathway and stimulates the proliferation of osteoblast-\like cells, *Bioelectromagnetics*, 2019, **40**(6), 412–421.

60 C. L. Ross, I. Syed, T. L. Smith and B. S. Harrison, The regenerative effects of electromagnetic field on spinal cord injury, *Electromagn. Biol. Med.*, 2017, **36**(1), 74–87.

61 Y. Zhang, W. Li, C. Liu, J. Yan, X. Yuan, W. Wang, H. Wang, H. Wu and Y. Yang, Electromagnetic field treatment increases purinergic receptor P2X7 expression and activates its downstream Akt/GSK3β/β-catenin axis in mesenchymal stem cells under osteogenic induction, *Stem Cell Res. Ther.*, 2019, **10**, 1–13.

62 M. C. d Abreu, D. Ponzoni, R. Langie, F. E. Artuzi and E. Puricelli, Effects of a buried magnetic field on cranial bone reconstruction in rats, *J. Appl. Oral Sci.*, 2016, **24**, 162–170.

63 J. Chen, C. Tu, X. Tang, H. Li, J. Yan, Y. Ma, H. Wu and C. Liu, The combinatory effect of sinusoidal electromagnetic field and VEGF promotes osteogenesis and angiogenesis of mesenchymal stem cell-laden PCL/HA implants in a rat subcritical cranial defect, *Stem Cell Res. Ther.*, 2019, **10**(1), 379.

64 N. Bloise, A. Patrucco, G. Bruni, G. Montagna, R. Caringella, L. Fassina, C. Tonin and L. Visai, In vitro production of calcified bone matrix onto wool keratin scaffolds via osteogenic factors and electromagnetic stimulus, *Materials*, 2020, **13**(14), 3052.

65 S. Ghodbane, A. Lahbib, M. Sakly and H. Abdelmelek, Bioeffects of static magnetic fields: oxidative stress, genotoxic effects, and cancer studies, *BioMed Res. Int.*, 2013, **2013**, 602987.

66 X. Zhang, *Biological effects of static magnetic fields*, Springer Nature, 2023.

67 C. Ma, H. Wang, Y. Chi, Y. Wang, L. Jiang, N. Xu, Q. Wu, Q. Feng and X. Sun, Preparation of oriented collagen fiber scaffolds and its application in bone tissue engineering, *Appl. Mater. Today*, 2021, **22**, 100902.

68 A. Rasch, H. Naujokat, F. Wang, A. Seekamp, S. Fuchs and T. Klüter, Evaluation of bone allograft processing methods: Impact on decellularization efficacy, biocompatibility and mesenchymal stem cell functionality, *PLoS One*, 2019, **14**(6), e0218404.

69 M. J. Eagle, P. Rooney and J. N. Kearney, Optimized demineralization of human cancellous bone by application of a vacuum, *J. Biomed. Mater. Res., Part B*, 2015, **103**(5), 1023.

70 K. Roshanbinfar, J. Hilborn, O. P. Varghese and O. P. Oommen, Injectable and thermoresponsive pericardial matrix derived conductive scaffold for cardiac tissue engineering, *RSC Adv.*, 2017, **7**(51), 31980–31988.

71 G. Borciani, G. Montalbano, N. Baldini, C. Vitale-Brovarone and G. Ciapetti, Protocol of co-culture of human osteoblasts and ost, *Methods Protoc.*, 2022, **5**(1), 8.
72 K. Roshanbinfar, L. Vogt, B. Greber, S. Diecke, A. R. Boccaccini, T. Scheibel and F. B. Engel, Electroconductive biohybrid hydrogel for enhanced maturation and beating properties of engineered cardiac tissues, *Adv. Funct. Mater.*, 2018, **28**(42), 1803951.
73 X.-J. Tang, K.-M. Huang, H. Gui, J.-J. Wang, J.-T. Lu, L.-J. Dai, L. Zhang and G. Wang, Pluronic-based micelle encapsulation potentiates myricetin-induced cytotoxicity in human glioblastoma cells, *Int. J. Nanomed.*, 2016, 4991–5002.
74 S. Shahriarpanah, J. Nourmohammadi and G. Amoabediny, Fabrication and characterization of carboxylated starch-chitosan bioactive scaffold for bone regeneration, *Int. J. Biol. Macromol.*, 2016, **93**, 1069–1078.